Supporting Information for

Sequential Activation of Spatially Localized Oligonucleotides

Moshe Rubanov[a], Phillip J. Dorsey[a], Dominic Scalise[a] and Rebecca Schulman[a,b,c]*

[a]Department of Chemical and Biomolecular Engineering, Johns Hopkins University, 3400 N. Charles Street, Baltimore, Maryland 21218, United States

[b]Department of Computer Science, Johns Hopkins University, 3400 N. Charles Street, Baltimore, Maryland 21218, United States

[c]Department of Chemistry, Johns Hopkins University, 3400 N. Charles Street, Baltimore, Maryland 21218, United States

*Email: rschulm3@jhu.edu (Rebecca Schulman)

Table of Contents

Section S1: *Sequential activation circuit design.* The circuit was designed by modifying a sequential activation reaction cascade studied in *Scalise et al.*[1]. Acrydite moieties were added to the Threshold and Payload complexes used in that work so that these complexes could be copolymerized within PEG hydrogels. The sequence of the bottom strand of each Payload complex (the strand with a fluorophore modification on the 5' end) was extended by adding a 20-base pair sequence to its 3' end complementary to an acrydite-labeled strand. All circuit components, with colored domains depicting the same sequences, are shown in **Figure S1**. Sequences are listed in **Table S2**.

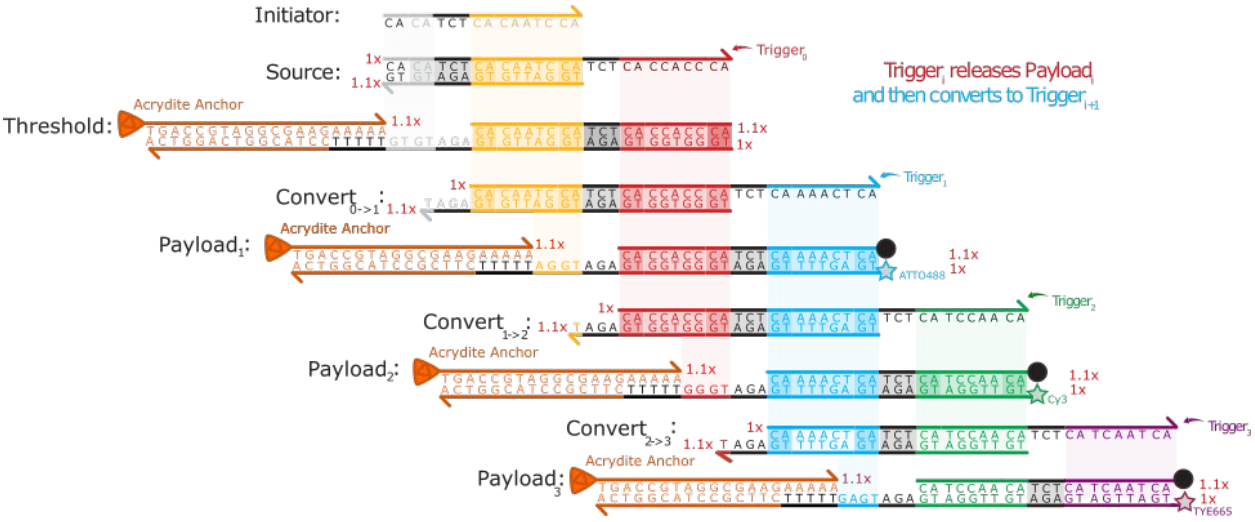

Figure S1: The components of the sequential activation circuit studied in this work. The strands were annealed with excess top or bottom strand, with the proportions denoted in red text on the side of either strand. For example, Source was annealed with 1x of the top strand, and 1.1x of the bottom strand, following the annealing protocol detailed in **Section S2a**.

Section S2: *Selection of concentrations of sequential activation circuit components*

The concentrations of the species of the 3-stage sequential activation circuit, as studied in well-mixed solution, simulated in COMSOL models **(Figure 3d, e)**, and used in Payload-embedded hydrogel sequential activation experiments **(Figure 4)** were calculated as shown below.

We wanted to design a circuit whose release schedule extended over hours to days to emulate biological timescales. For this reason, the timescale of the Trigger Production reaction, a bimolecular reaction between Source and Initiator, that provides the free energy required to power the rest of the chemical reaction network, had to be on the order of several days. A zero-base pair reaction in which the Source and Initiator react without a toehold, can persist for days when the initial concentrations of Source and Initiator are on the scale of micromolar. Additionally, if the concentrations of Source and Initiator are high enough, these reactants can act as a large reservoir, *i.e.,* their concentrations also do not change appreciably over days. This characteristic enables the reaction to emulate 0^{th} order reaction kinetics, which yields an approximately linear rate of Trigger production (*i.e.* release) over time when using high initial reactant concentrations[1]. To generate a constant rate of Trigger production over tens of hours using approximate 0^{th} order reaction kinetics, we chose Source and initiator concentrations of 2 μM.

We also sought to study spatiotemporal activation of the stages in the network using fluorescence microscopy. To measure the dynamics of activation on a standard wide field enabled inverted microscope, we had to determine the concentration regime of Payload that would provide a

robust signal to background noise ratio when imaged within hydrogels patterned on our microfluidic apparatus. We patterned cylindrical hydrogels of 150 µm diameter and 100 µm height with varying concentrations of fluorescently labeled DNA and observed that 100 nM Payload concentration provided a well-defined intensity profile. Conversely, Payload concentrations of 25 nM yielded fluorescence intensities that were too low to reliably measure the degree of Payload activation above the background intensity. We chose a Payload concentration of 100 nM in each stage for this study. Since the threshold acts as the 0^{th} stage Payload, we set the concentration of the Threshold to 100 nM as well.

We set the concentration of the Convert complex for each stage according to *Scalise et al.*[1] which detailed a protocol in which the Convert concentration used is 1.5x the total required amount of downstream Trigger for all subsequent stages. The Convert concentrations for stage *i* in an n-stage circuit can be written as:

$$[1]\ C_{i\rightarrow i+1} = 1.5[P](n-i)$$

where [P] is the Payload concentration, *i* is the stage number (the threshold stage is the 0^{th} stage), and *n* is the total number of stages. Specifically, for a 3-stage sequential activation circuit that uses 100 nM Threshold and 100 nM Payloads for each stage, the Convert concentrations are:

$$[2]\ C_{0\rightarrow 1} = 450\ nM,\ C_{1\rightarrow 2} = 300\ nM, C_{2\rightarrow 3} = 150\ nM$$

Section S3: *Purification protocol for reactant components.*

We ordered all strands for the sequential activation circuit from IDT (Integrated DNA Technologies) using PAGE-purification to ensure no base deletions; 90% of the sequences were guaranteed to come without base deletions for PAGE purified strands. Complexes were annealed to find thermodynamic global minima using an annealing procedure where the sample is first heated to 90°C for 5 minutes, then cooled to 20°C slowly, decreasing by 1°C per minute in an Eppendorf Mastercycler. Certain strands were annealed with 1.1x excess (10% excess compared to the complements in the complex) as shown on the end of each strand in **Figure S1**. The strands that were involved in triggering the subsequent stage, or the fluorescent strands in the Payloads that bound to the trigger strands, are annealed at 1x compared to their respective complements.

Section S4: *Further purification of DNA complexes*

In *Scalise et al.*[1]*,* the complexes were further purified using PAGE-purification to remove unannealed strands. However, due to the time-consuming nature of DNA complex PAGE-purification, we believed that we could use unpurified complexes while still achieving the qualitative behavior of activation between the three stages. Therefore, we purchased IDT PAGE-pure single strands (annealing protocol discussed in **Section S2a**), but ran the experiments shown in **Figure S2b** without further complex purification, but with identical concentrations that were used in the 4-stage sequential activation circuit in *Scalise et al.*[1]. When removing complex purification, we observed the 4-stage sequential activation circuit had differing kinetics compared to the 4-stage sequential activation circuit in *Scalise et al.*[1] with significant overlap between the first and second Payload activation timings. We additionally observed that Payloads 2-4 had separation between activation of each stage – there were approximately 5-hour separations between the 50% activation of each stage. For this reason, we decided not to monitor the fluorescence levels of $Payload_1$, and instead focus on the subsequent 3 stages. The sequences of our resulting circuit were thus named Threshold, $Payload_1$, $Payload_2$, and $Payload_3$.

Reactant	Figure S2a,	Figures S2b, 3d (nM)	Figures 3e, 4, S7, S9, S10, S11 (nM)	Figure S8 (nM)
Source	1000	2000	2000	2000
Initiator	1000	2000	2000	2000
Threshold	25	100	100	100
Damper Payloads 1-3	0	0	100	D_1: 50, D_2: 25, D_3: 0
Payloads 1-3	25	100	100	P_1: 50, P_2: 75, P_3: 100
$Convert_{01}$	112.5	450	450	450
$Convert_{12}$	75	300	300	300
$Convert_{23}$	37.5	150	150	150

Table S1: Reactant concentrations for each figure.

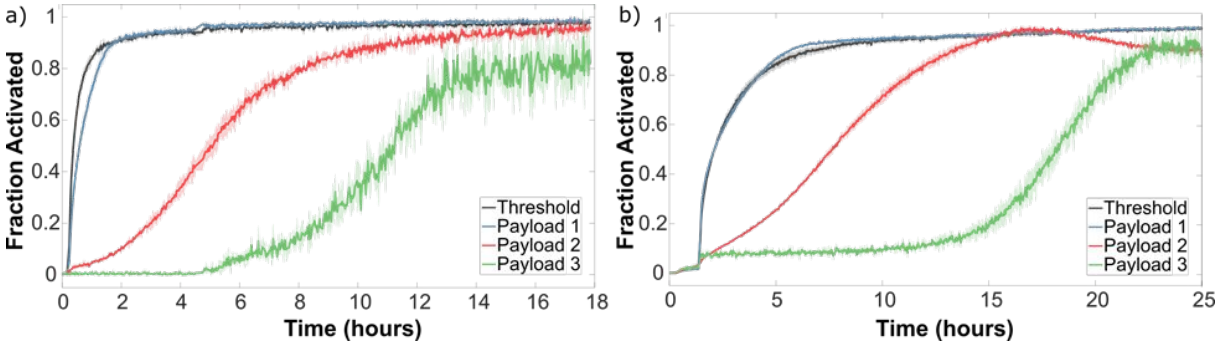

Figure S2: Kinetics of the sequential activation circuit in well-mixed solution plotted as fraction activated vs time. a**)** The kinetics of the sequential activation circuit where the concentrations of the Payload and Threshold complexes are each 25 nM; the strands making up the complexes were PAGE-purified, but the complexes themselves were annealed and not purified further. Significant overlap in the release times between the first two stages indicates significant leak (*i.e.* unintended reactions) occurs when using impurely annealed complexes (for the Payload and convert molecules). **b)** The same purification protocol as in (a) using 100 nM of each of the Payload and Threshold complexes. $Payload_1$ is activated by about 5 hours; and there are roughly 10 hours between the activation times for each subsequent Payload. All samples were run with at least three replicates. The means at each time point are plotted in the solid line and the standard deviations are shown as shaded regions above and below the solid lines. The concentrations of all components are listed in **Table S1**.

Section S5: *Reaction-diffusion model development.* Modeling of the spatiotemporal progression of the sequential activation network was done using finite element analysis in COMSOL 5.1 using approximate rate constants from *Zhang et al*[2]. The chemical reactions implemented in the model were the following:

$$S + I \xrightarrow{k_{0BP}} T_1$$

$$P_{1D} + T_1 \xrightarrow{k_{7BP}} F_{1D} + Q_1$$

$$C_{12} + T_1 \xrightarrow{k_{4BP}} T_2$$

$$P_{2A} + T_2 \overset{k_{7BP}}{\rightarrow} F_{2A} + Q_2$$

$$P_{2D} + T_2 \overset{k_{7BP}}{\rightarrow} F_{2D} + Q_{2D}$$

$$C_{23} + T_2 \overset{k_{4BP}}{\rightarrow} T_3$$

$$P_{3A} + T_3 \overset{k_{7BP}}{\rightarrow} F_{3A} + Q_3$$

$$P_{3D} + T_3 \overset{k_{7BP}}{\rightarrow} F_{3D} + Q_{3D}$$

$$C_{34} + T_3 \overset{k_{4BP}}{\rightarrow} T_4$$

$$P_{4A} + T_4 \overset{k_{7BP}}{\rightarrow} F_{4A} + Q_4$$

$$P_{4D} + T_4 \overset{k_{7BP}}{\rightarrow} F_{4D} + Q_{4D}$$

Where S = Source, I = Initiator, T_i= trigger i, P_{iD}= Damper Payload (dPayload) i, $C_{i,i+1}$= Convert $i \rightarrow i+1$, P_{iA} = anchored Payload (Payload) i, Q_i= Quencher i, Q_{iD}= dPayload quencher (waste product) i, where i is the stage number (1-4). The values for the three rate constants used were $k_{0BP} = 0.5\frac{L}{mol*s}$, $k_{4BP} = 5*10^3\frac{L}{mol*s}$, $k_{7BP} = 3*10^6\frac{L}{mol*s}$

These constants were placed into a system of ordinary differential equations:

$$[4]\ \frac{dS}{dt} = \frac{dI}{dt} = -k_{0BP}SI$$

$$[5]\ \frac{dT_1}{dt} = k_{0BP}SI - k_{7BP}P_{1D}T_1 - k_{4BP}C_{12}T_1$$

$$[6]\ \frac{dC_{12}}{dt} = -k_{4BP}C_{12}T_1$$

$$[7]\ \frac{dT_2}{dt} = k_{4BP}C_{12}T_1 - k_{7BP}P_{2A}T_2 - k_{7BP}P_{2D}T_2 - k_{4BP}C_{23}T_2$$

$$[8]\ \frac{dP_{2A}}{dt} = -\frac{dF_{2A}}{dt} = -k_{7BP}P_{2A}T_2$$

$$[9]\ \frac{dP_{2D}}{dt} = -\frac{dF_{2D}}{dt} = -k_{7BP}P_{2D}T_2$$

$$[10]\ \frac{dC_{23}}{dt} = -k_{4BP}C_{23}T_2$$

$$[11]\ \frac{dT_3}{dt} = k_{4BP}C_{23}T_2 - k_{7BP}P_{3A}T_3 - k_{7BP}P_{3D}T_3 - k_{4BP}C_{34}T_3$$

$$[12]\ \frac{dP_{3A}}{dt} = -\frac{dF_{3A}}{dt} = -k_{7BP}P_{3A}T_3$$

$$[13]\ \frac{dP_{3D}}{dt} = -\frac{dF_{3D}}{dt} = -k_{7BP}P_{3D}T_3$$

$$[14]\ \frac{dC_{34}}{dt} = -k_{4BP}C_{34}T_3$$

$$[15]\ \frac{dT_4}{dt} = k_{4BP}C_{34}T_3 - k_{7BP}P_{4A}T_4 - k_{7BP}P_{4D}T_4$$

$$[16]\ \frac{dP_{4A}}{dt} = -\frac{dF_{4A}}{dt} = -k_{7BP}P_{4A}T_4$$

$$[17]\ \frac{dP_{4D}}{dt} = -\frac{dF_{4D}}{dt} = -k_{7BP}P_{4D}T_4$$

$$[18]\ \frac{dQ}{dt} = k_{7BP}P_{1A}T_1 + k_{7BP}P_{2A}T_2$$

$$[19]\ \frac{dQ_D}{dt} = k_{7BP}P_{1D}T_1 + k_{7BP}P_{2D}T_2$$

This system of ordinary differential equations was modeled in COMSOL as a system of partial differential equations. Each ODE was modified to include a diffusion term and is calculated at each location in 2D space. For example, in equation [4], the ODE was modified into a PDE:

$$[20]\ \frac{\partial S(t,x,y)}{\partial t} = D_S\nabla^2 S - k_{0BP}SI$$

The initial conditions vary depending on the experiment we tried to model from **Figure 3**. The models in **Figure 3** used a geometry defined as three 150 μm-radius circles. Each circle represents a single-domain hydrogel that can anchor different chemical reaction cascade components within that domain. We model the anchoring of chemical components by assigning those components a diffusion constant of 0 μm²/s, whereas freely diffusing components have diffusion coefficients of 60 μm²/s in the hydrogels (modeled as circles), and 150 μm²/s elsewhere. The spatially averaged concentration of each of these circles was subsequently plotted and displayed both in **Figures 3d, e, S8-S11.**

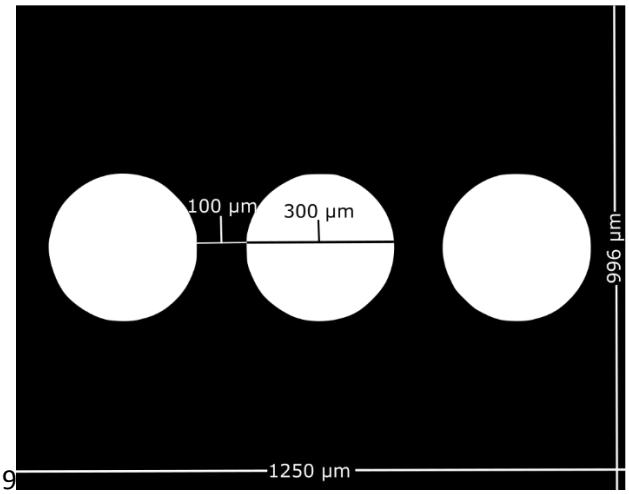

Figure S3: Geometry used in the model. The white portions are the circular hydrogels, and the black portion is the surrounding solution. The results of the simulations performed using this geometry are presented in **Figure 3d,e**, **Figures S7-S11.**

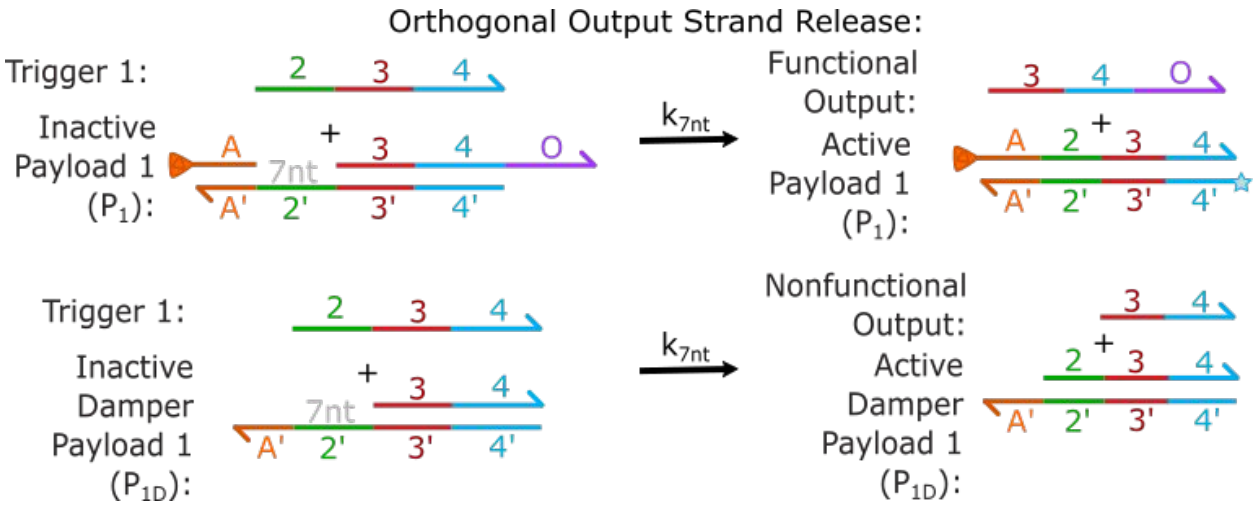

Figure S4: A scheme for Output strand release where "functional" outputs have different potential for downstream reactivity than "nonfunctional" outputs. An output domain 'O' becomes available for downstream reactions that use unique sequences not found in the sequential activation circuit (such as an aptamer binding domain) at specific locations where the Payload is anchored. Although there are damper Payloads undergoing similar reactions in the surrounding solution, since the damper Payload has no output strand, this schematic demonstrates a potential way of localizing an output domain while maintaining the circuit kinetics as described in **Figure 3e.**

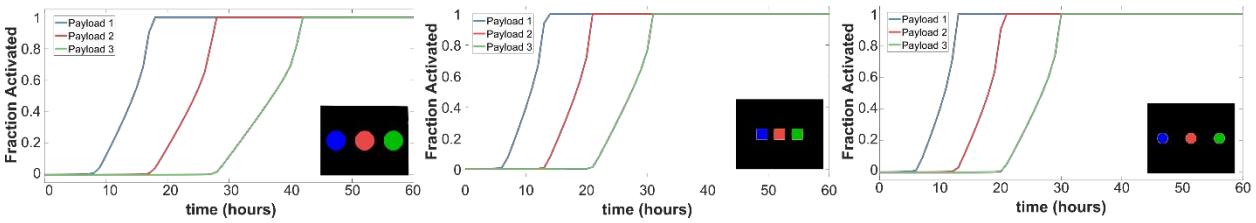

Figure S5: The kinetics of activation for different hydrogel geometries as predicted in models. The first profile shows 300 µm diameter cylinders, the second plot shows 150 µm-side rectangular posts, and the third profile shows 150 µm diameter cylinders. The circles were 400 µm apart (center to center), while the squares were 250 µm apart (center to center).

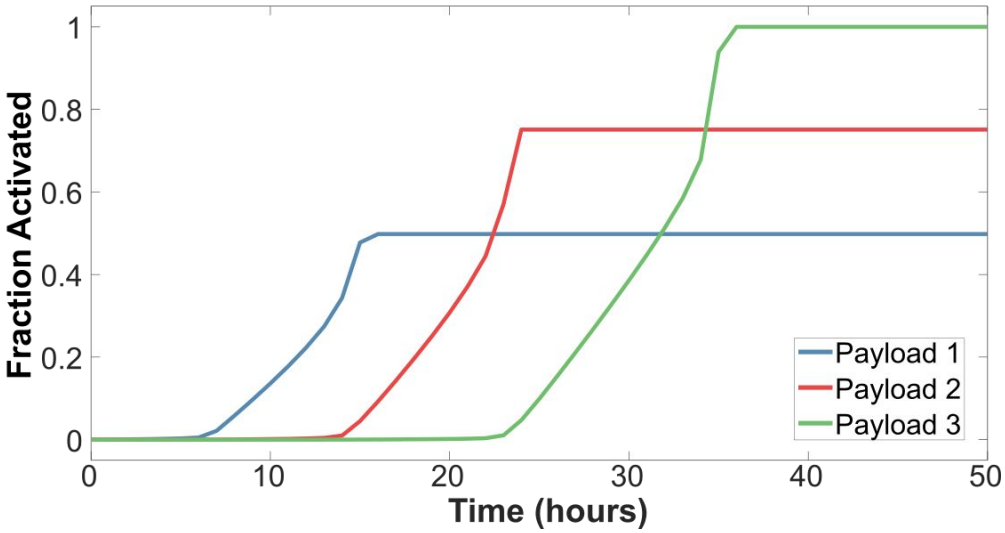

Figure S6: Partial Payload Activation. When replacing the anchored payload within each hydrogel with a fraction of Damper Payload in our simulations, the model predicts that we can modulate total fraction activated for each Payload without affecting kinetics. Payload 1, Payload 2, and Payload 3 were initialized with 50%, 75%, and 100% ratios of Payload to Damper Payload, respectively. Table S1 contains the concentrations for all reactants.

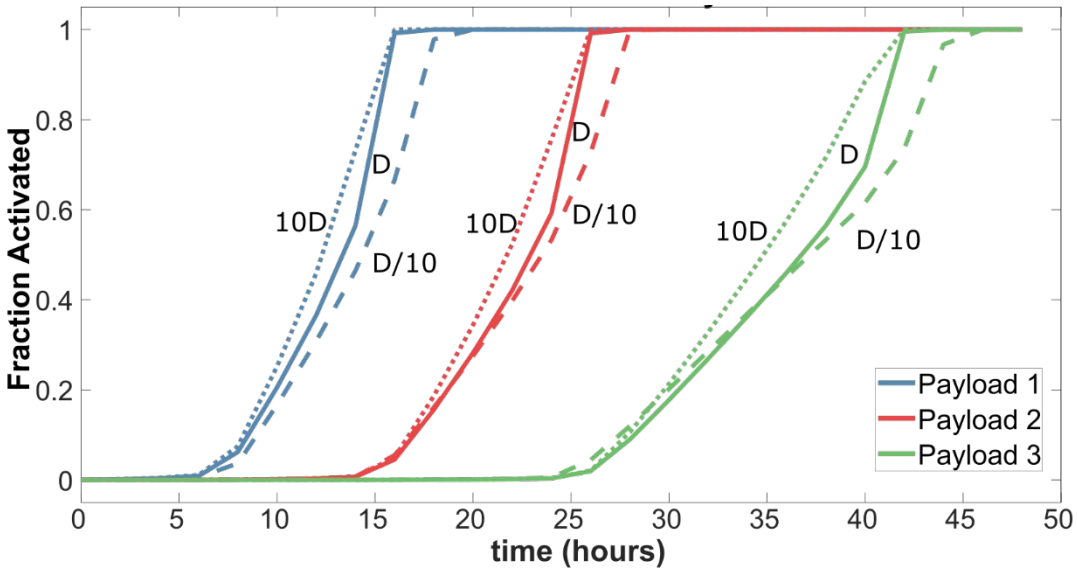

Figure S7: Modeling predicts that changes in diffusion coefficients of DNA complexes and strands do not significantly affect the activation profiles. The diffusion coefficients for both single stranded and double stranded DNA in the hydrogel were increased and decreased by an order of magnitude. The '10D' curves shows the activation profile for the reaction-diffusion model run with diffusion rates for Source, Initiator, and Convert complexes ten times larger than those used in the model presented in Section S5(600 $\mu m^2/s$ within the hydrogel and 1500 $\mu m^2/s$ outside the hydrogel), the 'D' curve shows the activation profile for the diffusion coefficients (based on prior measurements) used in the model in Section S5 (60 $\mu m^2/s$ within the hydrogel and 150 $\mu m^2/s$ outside the hydrogel), and 'D/10' curve shows the activation profile for diffusion coefficients ten times slower than those in the model presented in Section S5 (6 $\mu m^2/s$ within the hydrogel and 15 $\mu m^2/s$ outside the hydrogel). We observed that the activation profiles for the Payloads changed negligibly when the diffusion coefficients were changed dramatically: the times at which 50% of each Payload were activated changed by no more than 2 hours when the diffusion coefficient was either increased or decreased tenfold.

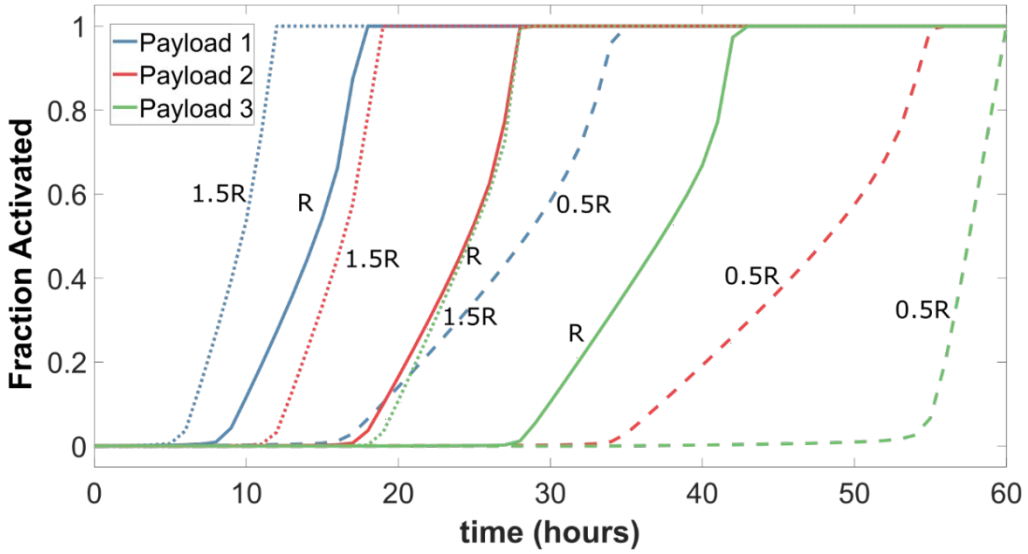

Figure S8: Modeled effect on activation time of changing the reaction rate constants for the sequential activation cascade. The reaction rate constants used in Figure 3d,e and as described in Section S5 are indicated by 'R' labels and solid lines. Coarsely dashed lines, with '0.5R' labels, show the results from the reaction-diffusion model when 0-,4-, and 7-nucleotide rates were 50% smaller than the values presented in Section S5. Finely dashed lines, with '1.5R' labels, show the results from the reaction-diffusion model when 0-,4-, and 7-nucleotide rates were 50% smaller than the values presented in Section S5. We observed that either increasing or decreasing all the reaction rate constants for the 0-,4-, and 7-nucleotide reactions by 50% drastically alters the activating profiles. The times at which 50% activation was achieved for the R curves were 5 hours apart, but the times at which 50% activation was achieved for the 0.5R curves were approximately 20 hours apart.

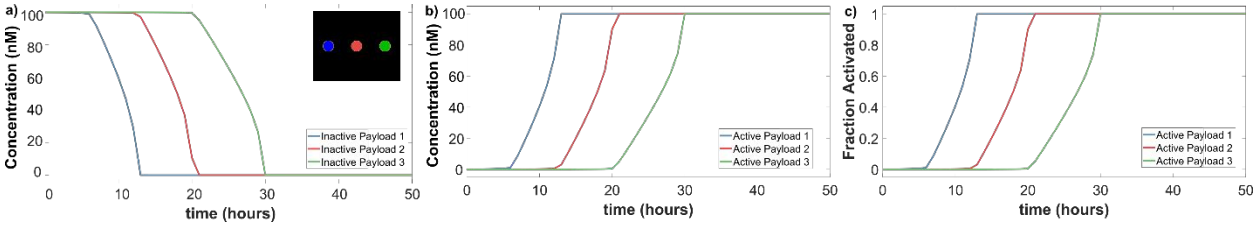

Figure S9: Method by which the activation of Payloads within hydrogel domains predicted by models was compared to results from experiments. We processed the COMSOL model data to compare the model to our experiments **(Figure 4)** by first measuring calculated the active Payload concentrations and then normalizing by dividing these concentrations by the total Payload concentration. Initially, the model computes both the active and inactive payload concentrations, which sum to 100 nM at a given time point ($P_{inactive} + P_{active} = 100$ nM) (**a** and **b**) after which we can normalize the active Payload plot in **b** with respect to the maximum initial Payload concentration (100 nM) to achieve the plot shown in **c**, which can be compared to the normalized experimental data. The COMSOL model geometry used for all three plots is shown in **a**.

Section S6: *Photopatterning of hydrogels and fabrication of microfluidic devices.* We adopted the method from *Dorsey et al.*[3] for fabrication and patterning of multi-domain hydrogels. In our workflow, different Payloads and Threshold were sequestered in different locations within hydrogel domains using

multistep, sequential patterning with a digital micromirror device (DMD) inside a microfluidic flow cell. Binary images were created and uploaded to the DMD (Mightex Polygon 400) and illuminated inside a microfluidic flow cell. The microfluidic flow cell was fabricated as detailed in *Dorsey et al*[3]. with dimensions of 10 mm (length), 1 mm (width), and 100 µm (height) **(Figure S12a)**. 200 nM of either Payload, damper Payload, or Threshold (refer to Table S1 for final concentrations inside each hydrogel) were added to a pregel solution consisting of: 10% v/v PEGDA-575 (Sigma-Aldrich, 437411), 3% v/v Omnirad 2100 (IGM Resins), and 1xTAEM buffer (40 mM Tris, 20 mM Acetic Acid, 1mM EDTA (Invitrogen, 24710030), 12.5 mM MgCl) in a total volume of 1 mL. The pregel solution for one hydrogel domain was injected into a microfluidic flow cell (**Figure S12a**) and subsequently photopatterned at different locations using an American Greenspot UV curing system for 5 seconds with a peak UV output of 7 watts for a total dosage across the DMD of approximately 140 J/mm^2. Between patterning steps, unused pregel solution was washed out of the cell by flowing in 1 mL of Butanol followed by 1 mL of 1xTAEM. We tested this protocol by patterning 3-domain hydrogel sequentially (one hydrogel cylinder followed by 2 hydrogel rings), each containing different DNA Payloads labeled with distinct fluorescent dyes (**Figure S12b**). Hydrogel domains formed according to the designed binary image masks (shown in **Figure S12b i,ii,iii**).

In some cases, the edges of a hydrogel domain appeared brighter than its center. We hypothesize that the edges of a domain remain brighter due to an observed phenomena that occurs when photopolymerizing hydrogels at the length scales (100 µm) and timescales (seconds) that we use. The brighter edges are caused by a higher crosslink density of monomer, and therefore increased concentration of acrydite-labeled DNA near the edges. For hydrogel photopolymerization where the monomer takes longer to diffuse across the illuminated region than the total exposure time, more densely crosslinked edges are observed since the monomers can constantly diffuse into the edge of the illuminated region and react with the photoinitiator during the UV exposure. When highly crosslinked hydrogel edges are observed, the process is classified as a reaction-dominated regime since the photopolymerization reaction takes place non-uniformly based on the limited diffusivity of the monomer across the region coupled with longer exposure times (on the order of seconds)[4]. When we compare the uniformity of hydrogel fluorescence by analyzing the red fluorescent profile across a multi-domain hydrogel (**Figure S12**), we observed higher fluorescence on the edges as compared to the center of the hydrogel. In this case, when observing the red hydrogel ring, the outer edge is brighter than the internal edge due to the contact the outer edge has with the pre-gel solution, allowing for influx of the monomer, while the internal hydrogel cylinder prevents diffusing new pregel solution into the inner edge during the UV exposure.

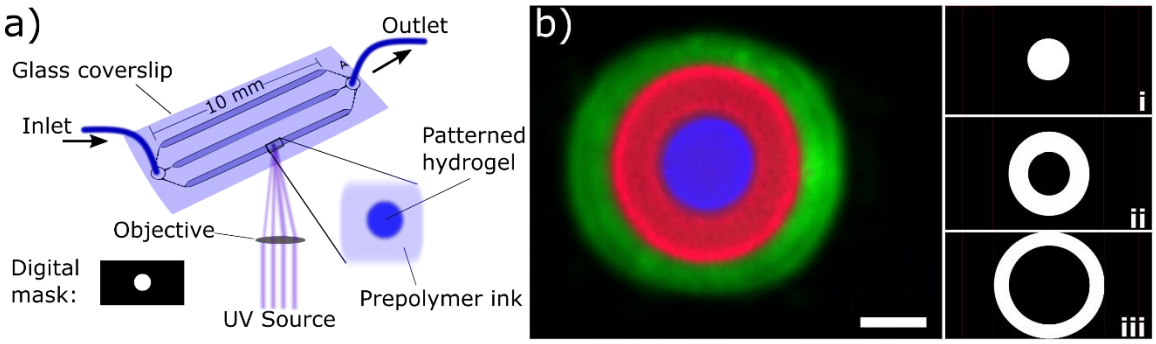

Figure S10: Photopatterning of Payload-containing hydrogels. **a)** The microfluidic chamber used for creating the multi-domain hydrogel. For this device, the pregel solution was flowed into the inlet, patterned using a digital mask created in a digital micromirror device (DMD), and subsequently washed out. **b)** A 3-domain hydrogel using digital lithography. Each domain contains a unique fluorophore patterned using the masks shown (**i, ii, iii**). The blue domain was patterned using mask **i**, the red domain using mask **ii,** and the green domain using mask **iii.**

Section S7: *Acrydite-modified DNA retention calculation.* We measured the fraction of DNA in the pregel solution that becomes anchored to the polymer network during photopolymerization. We then used the fraction incorporated to design pregel solutions that would incorporate the desired concentration of Threshold and Payload complexes into the hydrogels post-photopolymerization. We used a simple acrydite retention experiment that compared the fluorescence of a DNA-crosslinked PEGDA hydrogel right after patterning to the fluorescence after washing away the fluorescent pregel solution. DNA anchoring (or retention) was quantified by photopolymerizing 200 nM of acrydite-tagged, Cy3-labeled fluorescent DNA complex, Payload 3 without the hybridized quencher strand, termed P3FA which stands for Payload 3_Fluorophore_Quencher (**SI Table S2** for sequences), into a PEGDA hydrogel inside a microfluidic flow cell. The fluorescence count level measured after 17mL of 1xTAE Mg^{2+} was flowed through the microfluidic flow cell using a syringe pump programmed for a flow rate of approximately 1 mL/hr was compared with the initial fluorescence counts of the hydrogel directly after photopolymerization in the pregel solution. We then calculated the percent retained (N) as

$$[20]\ N = \frac{R - dark}{start - dark}$$

where

- *R* is the raw fluorescent intensity of the hydrogel, averaged over the area of the hydrogel
- *dark* is the estimated background fluorescence intensity of a hydrogel in the image, *i.e.* the measured fluorescence intensity of a hydrogel containing no fluorescent DNA, averaged over the hydrogel area
- *start* is *R* at t=0.

Intensity was measured as fluorescent counts captured by the camera. The percent retained for 3 replicate hydrogels after 17 hours was $55 \pm 3.9\%$ (mean $\pm$ s.d). Given that approximately 50% of the DNA in the pregel solution was incorporated into the hydrogel, we therefore assumed that we could achieve a specific concentration of DNA complexes attached to the hydrogel by adding roughly double that concentration of the DNA complex to the pregel solution. That is, to form hydrogels containing 100 nM of Threshold complex, we photopolymerized a pregel solution containing 200 nM of the complex. The same ratios of species were used for hydrogels containing each of the Payload Complexes.

PEGDA was used as the polymer forming hydrogels in this study. PEGDA is biocompatible and stable over days to weeks[5–8]. PEGDA-DNA functionalized hydrogels are well-studied, and have demonstrated conjugation of DNA up to 300 µM[9]. The observed ~50% fraction of DNA retained during hydrogel polymerization in Figure *S11* is thus likely limited by incomplete conjugation of the acrydite-modified DNA to the PEGDA backbone.

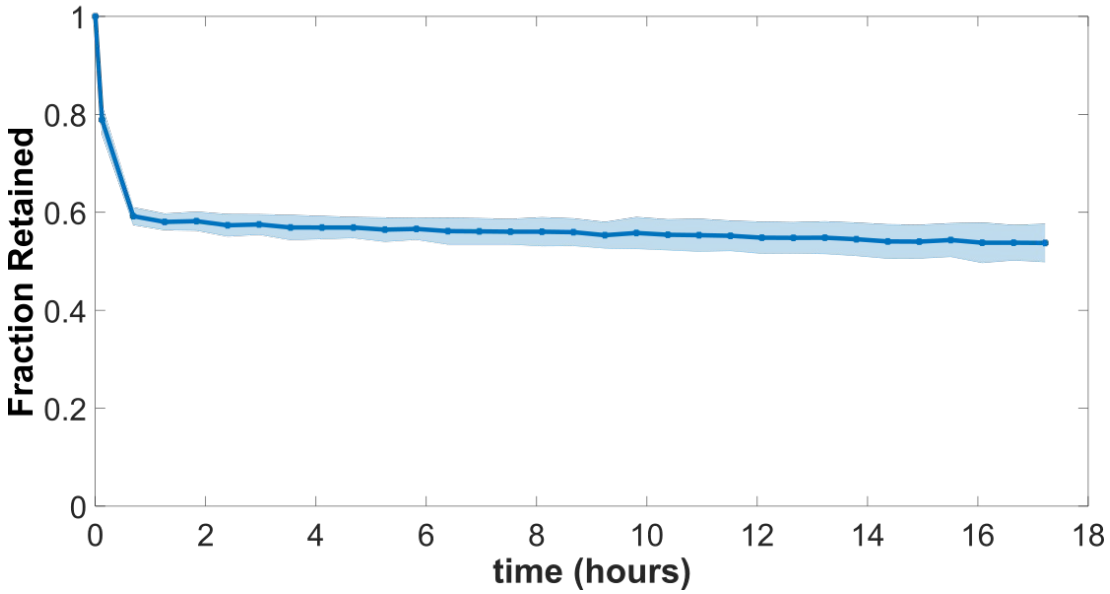

Figure S11: Acrydite and fluorophore-modified DNA (Cy3) retention within photopatterned hydrogels. This experiment was performed by first photopatterning a pregel solution containing 100 nM $Payload_3$ annealed without the quencher strand (Payload 3 without the hybridized quencher strand, or P3FA). We then measured the fluorescence within the hydrogel after washing the pregel solution surrounding the photopatterned hydrogel away. The wash consisted of 17 mL of 1xTAEM buffer solution over 17 hours. The retention rate was measured by analyzing the changes in fluorescence for three hydrogels patterned within the microfluidic device. The retention rate measured (N=3) was 55 ± 3.9% (mean ± s.d.). The shaded error bars surrounding the average line enclose the standard deviation across the mean measurement at time point. Retention percent was measured as described in Section S7.

Section S8: *Data processing for fluorescence plots.* We quantified the fluorescence microscopy data from **Figure 4b-d** by creating three binary image masks for each of the three image channels that capture the fluorescence of the three fluorophores within the multi-domain hydrogels. Each binary mask consisted of a 1 for pixels of an image that corresponded the hydrogel containing Payloads labeled with each of the three fluorophores and 0s for all other pixels. These image masks were used to isolate the pixels in each micrograph that correspond to each hydrogel domain, which could then be analyzed for intensity at each time point taken.

To measure each hydrogel's fluorescence intensity in a fluorescence micrograph, we multiplied each pixel in the fluorescence micrograph containing the raw fluorescence intensities by the corresponding pixel in the binary mask to create a resulting matrix in which the fluorescence intensities at all locations outside one of the hydrogels were 0. The nonzero pixel counts of this matrix were then averaged to measure the mean hydrogel domain intensity. The process of binary mask multiplication and averaging was applied to every image in the set (for each time point taken).

The fluorescence intensity data for each channel *N* was then normalized by taking the maximum and minimum average intensities of the hydrogels over the micrographs for all of the time points, and applying the following formula:

$$[21]\ N = \frac{R - min}{max - min}$$

where R is the average intensity of the raw image, min is the average intensity of the darkest image (the first image), max is the average intensity of the brightest image (the last image), and N is a normalized value representing the relative intensity between 0 and 1 for each time point.

The normalized values are plotted for each multi-domain hydrogel as shown in **Figure 4b-d**.

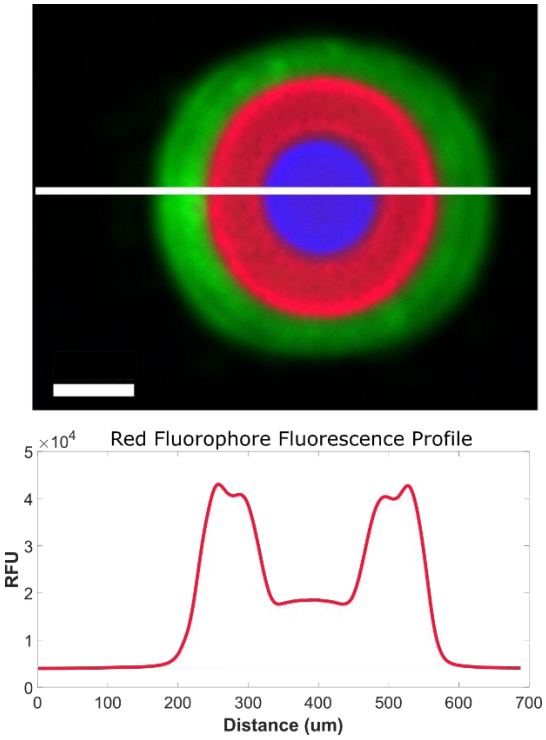

Figure S12: Hydrogel nonuniformity. The top image shows an example photopatterned hydrogel. The white bar in the top image shows a vector across which the fluorescence intensity of the red channel is plotted in bottom profile. Both the micrograph and fluorescence intensity profile show that the outer edge of the red domain is higher in fluorescence than the inner edge.

Section S9: Lack of *activation of the reaction network without source/initiator.*

To check whether the source and initiator were required to trigger the sequential release cascade, we ran the experiment described in SI Section S2 that measured the rate of Payload activation using a fluorescence-quencher assay in well-mixed solution using a plate reader, except that Source and Initiator were eliminated. That is, the concentrations of reagents were those shown in SI Table S1 except [Source]=[Initiator] = 0 nM. The results of this experiment are plotted in SI Figure S13. Almost no activation of any of the Payloads was observed within the 45 hour timespan of the experiment.

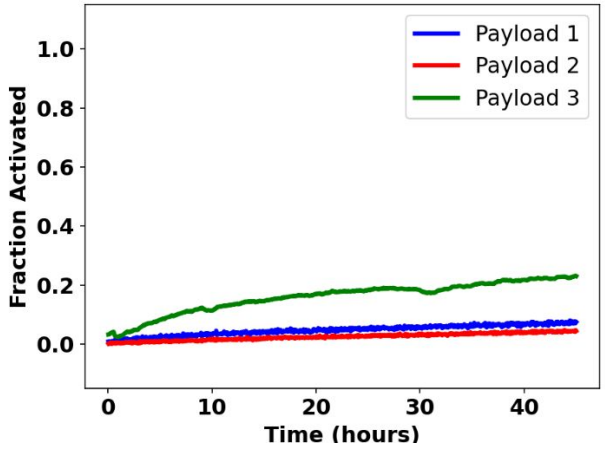

Figure S13: Kinetics of the sequential activation circuit without Source and Initiator in well-mixed solution plotted as fraction activated vs time. Threshold and Payload concentrations are 100 nM, Convert concentrations for $C_{1>2}$, $C_{2>3}$, $C_{3>4}$ are 450, 300, and 150 nM, respectively, and the Source and Initiator concentrations are 0 nM.

Section S10: *Threshold concentration influences Payload Activation Schedule.*

Here, we explore using simulations how the Threshold concentration influences the activation schedule of the 3 Payload activation stages. These simulations suggest that altering the Threshold concentration changes the time at which the first Payload is activated without changing the delay of activation of the subsequent Payloads.

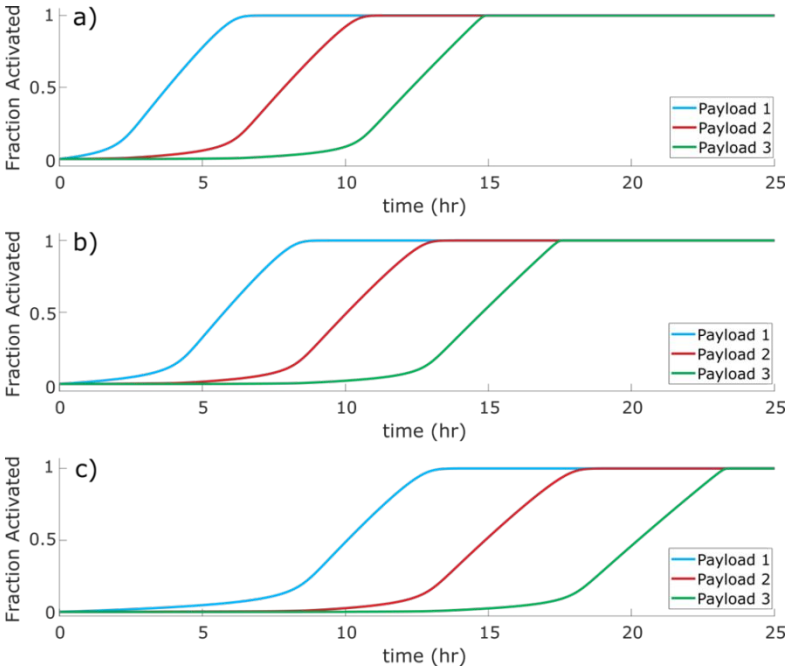

Figure S14: Results of simulations of Payload activation schedule for the sequential activation cascade at different concentrations of Threshold. The onset of Payload activation varies based on the Threshold

concentration. Here, we ran three models in well-mixed solution at varying concentrations of Threshold. Threshold values for each model were Threshold = 50, 100, 200 nM for a, b, and c, respectively.

Table S2: Circuit sequences

Convert0,1_Cover	CA CAATC CA TCT CA CCACC CA TCT CA AAACT CA
Convert0,1_Bottom	TG GGTGG TG AGA TG GATTG TG AGA T
Convert1,2_Cover	CA CCACC CA TCT CA AAACT CA TCT CA TCCAA CA
Convert1,2_Bottom	TG AGTTT TG AGA TG GGTGG TG AGA T
Convert2,3_Cover	CA AAACT CA TCT CA TCCAA CA TCT CA TCAAT CA
Convert2,3_Bottom	TG TTGGA TG AGA TG AGTTT TG AGA T
Threshold_CoverU	CA CAATC CA TCT CA CCACC CA
Threshold_BottomU	TG GGTGG TG AGA TG GATTG TG AGA TG TGT TTT TCT TCG CCT AC
Payload1_CoverU	CA CCACC CA TCT CA AAACT CA
Payload1_BottomU	TG AGTTT TG AGA TG GGTGG TG AGA TG GAT TTT TCT TCG CCT AC
Payload2_CoverU	CA AAACT CA TCT CA TCCAA CA
Payload2_BottomU	TG TTGGA TG AGA TG AGTTT TG AGA TG GGT TTT TCT TCG CCT AC
Payload3_CoverU	CA TCCAA CA TCT CA TCAAT CA
Payload3_BottomU	TG ATTGA TG AGA TG TTGGA TG AGA TG AG
Payload1_CoverQ_Atto488	CA CCACC CA TCT CA AAACT CA/3IABkFQ/
Payload1_BottomATTO488	/5ATTO488N/ TG AGTTT TG AGA TG GGTGG TG AGA TG GAT TTT TCT TCG CCT AC GGTCA
Payload2_CoverQSp	CA AAACT CA TCT CA TCCAA CA/3IABRQSp/
Payload2_BottomCy3 (probe for anchoring experiments)	/5Cy3 /TG TTGGA TG AGA TG AGTTT TG AGA TG GGT TTT TCT TCG CCT AC
Payload3_Cover3BHQ_2	CA TCCAA CA TCT CA TCAAT CA/3BHQ_2/
Payload3_bottomTYE665	/5TYE665/TG ATTGA TG AGA TG TTGGA TG AGA TG AG AGGTG CT TCG CCT AC GGTCA
Anchor Sequence	/5Acryd/TGA CCG TAG GCG AAG CACCT

References:

[1] D. Scalise, M. Rubanov, K. Miller, L. Potters, M. Noble, R. Schulman, Programming the Sequential Release of DNA, ACS Synth. Biol. 9 (2020) 749–755. https://doi.org/10.1021/acssynbio.9b00398.

[2] D.Y. Zhang, E. Winfree, Control of DNA Strand Displacement Kinetics Using Toehold Exchange, Journal of the American Chemical Society. 131 (2009) 17303–17314. https://doi.org/10.1021/ja906987s.

[3] P.J. Dorsey, M. Rubanov, W. Wang, R. Schulman, Digital Maskless Photolithographic Patterning of DNA-Functionalized Poly(ethylene glycol) Diacrylate Hydrogels with Visible Light Enabling Photodirected Release of Oligonucleotides, ACS Macro Lett. (2019) 1133–1140. https://doi.org/10.1021/acsmacrolett.9b00450.

[4] S. Park, D. Kim, S.Y. Ko, J.-O. Park, S. Akella, B. Xu, Y. Zhang, S. Fraden, Controlling uniformity of photopolymerized microscopic hydrogels, Lab Chip. 14 (2014) 1551–1563. https://doi.org/10.1039/C4LC00158C.

[5] S.J. Bryant, K.S. Anseth, Controlling the spatial distribution of ECM components in degradable PEG hydrogels for tissue engineering cartilage, Journal of Biomedical Materials Research Part A. 64A (2003) 70–79. https://doi.org/10.1002/jbm.a.10319.
[6] A. Mazzarotta, T.M. Caputo, L. Raiola, E. Battista, P.A. Netti, F. Causa, Small Oligonucleotides Detection in Three-Dimensional Polymer Network of DNA-PEG Hydrogels, Gels. 7 (2021) 90. https://doi.org/10.3390/gels7030090.
[7] Y.-C. Chiu, M.-H. Cheng, H. Engel, S.-W. Kao, J.C. Larson, S. Gupta, E.M. Brey, The role of pore size on vascularization and tissue remodeling in PEG hydrogels, Biomaterials. 32 (2011) 6045–6051. https://doi.org/10.1016/j.biomaterials.2011.04.066.
[8] P.J. Dorsey, D. Scalise, R. Schulman, DNA Reaction–Diffusion Attractor Patterns, Angewandte Chemie International Edition. 60 (2021) 338–344. https://doi.org/10.1002/anie.202009756.
[9] R.L. Srinivas, S.C. Chapin, P.S. Doyle, Aptamer-Functionalized Microgel Particles for Protein Detection, Anal. Chem. 83 (2011) 9138–9145. https://doi.org/10.1021/ac202335u.